Plasma Sources
Science and
Technology

PAPER • **OPEN ACCESS**

Modified state enhanced actinometry for measuring atomic oxygen density in a micro-scaled atmospheric pressure plasma jet

To cite this article: Kittawat Poonsawat and Erik Wagenaars 2025 *Plasma Sources Sci. Technol.* **34** 085009

OPEN ACCESS
IOP Publishing
Plasma Sources Science and Technology
Plasma Sources Sci. Technol. **34** (2025) 085009 (13pp)
https://doi.org/10.1088/1361-6595/adf666

Modified state enhanced actinometry for measuring atomic oxygen density in a micro-scaled atmospheric pressure plasma jet

Kittawat Poonsawat and Erik Wagenaars*

York Plasma Institute, School of Physics, Engineering and Technology, University of York, York YO10 5DD, United Kingdom

E-mail: erik.wagenaars@york.ac.uk

Received 12 December 2024, revised 30 May 2025
Accepted for publication 31 July 2025
Published 13 August 2025

Abstract

Plasma-produced oxygen atoms (O) are powerful oxidative radicals that play important roles in plasma-induced chemical modification of material surfaces. Measuring O density in plasmas is important to enhance our understanding and control. Two-photon absorption laser-induced fluorescence (TALIF) is widely used for measuring O density, but is experimentally complex and often incompatible with in-situ process control. Actinometry, based on analysing spectral lines from optical emission spectroscopy, requires only simple hardware, but relies on more complex analysis of experimental data. Advanced actinometry methods such as state enhanced actinometry (SEA) have recently been developed and are consistent with TALIF measurements. In this work, a modified version of SEA is investigated. Including cascading effects in the SEA analysis model and reducing the effect of metastable states on the SEA emission line by considering the 728.1 nm He($3\ ^1S \rightarrow 2\ ^1P$) line, instead of the 706.5 nm He($3\ ^3S \rightarrow 2\ ^3P$) line, are considered. Importantly, Bayesian inference is used for matching experimental and theoretical data from the non-linear equations of each model. O density and mean electron energy are determined in a micro-scaled atmospheric pressure plasma jet (μAPPJ), operated with 1 slm of He and admixtures of 0.5% O_2 and 0.1% Ar. It is found that the Bayesian process minimises the associated error to less than 1%. Both including cascading emission and considering the alternative He line result in significant changes to the derived O density, in the range of 20%–60% overall. However, because of the lack of accurate data from alternative methods, e.g. TALIF has an accuracy of 67% approximately, and the uncertainty of SEA itself ($\approx$20%), due to uncertainties in the parameters used in the models, it is not possible to

* Author to whom any correspondence should be addressed.

determine which model is the most appropriate for SEA and whether our modifications lead to improvements. The work highlights the currently achievable accuracy of advanced actinometry methods such as SEA.

Keywords: actinometry, low-temperature plasma, plasma diagnostic, plasma radicals

1. Introduction

Atmospheric pressure plasmas (APPs) have gained significant interest over recent years. APPs can be operated in open air without the need for a vacuum system, leading to a reduced operational complexity and cost. Moreover, APPs can deliver high densities of reactive species to a substrate while the gas temperature remains close to room temperature [1, 2]. Because of this, these plasmas have potential for various applications ranging from surface modifications [3–5], decontamination [6, 7], medicine [8, 9] and photoresist removal [10].

The effectiveness of a plasma treatment is often related to the mix of reactive species that is delivered to a substrate. As a result, knowing and controlling this mix of species is essential, but unfortunately complicated due to the many different reactive species that exist and the complex interactions between them. One of the reactive species of interest for many applications is atomic oxygen (O), produced from oxygen-containing plasmas. Not only does atomic oxygen have its own oxidative properties, but it also contributes as a precursor to the formation and decomposition of a variety of long-lived molecules, such as ozone [11].

Two-photon absorption laser-induced fluorescence (TALIF) [12–15] is a well-established method for directly measuring O density in a plasma. TALIF requires two photons from a laser system with a specific wavelength to excite ground-state atomic oxygen to an excited state. Fluorescence radiation is detected to quantify the atomic oxygen density. Calibration of this diagnostic with xenon gas allows the measurement of absolute O densities. Although TALIF can directly determine O density, it is complex in operation, expensive in hardware and often not compatible with plasma systems in real-life applications.

Actinometry is a promising method for determining O density for situations where TALIF is not appropriate. The concept was first published by Coburn and Chen [16], and it was first used for determining O density by Walkup *et al* [17]. It is a passive diagnostic that works by detecting optical emission from a plasma and using an analytic intensity model to calculate O density. The ratio of the emission of O and an actinometer gas, most commonly argon for O actinometry, is used in the analytical model to derive the O density. The concentration of the actinometer gas is kept low so that it does not change the plasma properties. The type of actinometer gas is chosen such that there is a transition that has a similar shape and energy threshold of the electron-impact excitation cross section as the transition observed in the plasma. The main assumptions of the method are that the excited state is populated only via electron-impact excitation from its ground state and de-excitation is only through spontaneous emission. This allows the O density to be determined from the intensity ratio of O and Ar emission lines, without needing information about the electron density (n_e) and the electron energy distribution function (EEDF) of the plasma. In practice, two O emission lines at the wavelengths of 777.4 nm ($O(3p\ ^5P \rightarrow 3s\ ^5S)$) and 844.6 nm ($O(3p\ ^3P \rightarrow 3s\ ^3S)$) as well as the Ar line at 750.4 nm ($Ar(2p_1 \rightarrow 1s_2)$) have been used for actinometry purposes. It was found that even though there was reasonable qualitative agreement, this method overestimated the O density when compared with TALIF.

Katsch *et al* [18] improved the actinometry method by including the processes of dissociative electron-impact excitation and collisional quenching in the analytical intensity model. It was found that adding these processes gave more accurate results, especially when using the 844.6 nm O emission line. For the 777.4 nm O emission line, there are concerns about the effect of population of the upper level through excitation from metastable states, resulting in an overestimation of the O density. The main drawback of this method is that it requires details of the EEDF to be known. For the low-pressure plasma in the study of Katsch *et al*, the EEDF could be modelled and compared with that obtained from a Langmuir probe measurement. This is often not possible for APPs.

Actinometry for an APP was proposed by Niemi *et al* [19, 20]. The EEDF of the plasma, needed for actinometry, was determined from diagnostic-based modelling. A numerical simulation based on fluid equations in 1 dimension was used to generate the EEDF [21]. The simulations were verified by comparing the simulated time and space resolved electron-impact excitation rate of the $Ar(2p_1)$, with the results from phase-resolved optical emission spectroscopy (PROES) measurements [22]. In order to quantify O density, the integrated intensity ratio between the 844.6 nm O emission line and the 750.4 nm Ar emission line was required. Furthermore, the time and space averaged electron density weighted EEDF was calculated from diagnostic-based modelling and used to calculate electron-impact excitation rate coefficients.

Subsequently, Greb *et al* [23] published a related technique called energy resolved actinometry (ERA) for an APP, which uses two excitation ratios. The ratio of excitation from the ground state to the $O(3p\ ^5P)$ and $Ar(2p_1)$ upper states, and the ratio between the excitation to the $O(3p\ ^3P)$ and $Ar(2p_1)$ upper states. By using two excitation ratios, both the O density and the mean electron energy of the plasma could be determined. The excitation ratios were measured with PROES and EEDFs for mean electron energy were simulated with BOLSIG+ [24]. This method gave good results for a micro-scaled APP jet (μAPPJ). However, the need for a more complex diagnostic such as PROES instead of a simpler OES makes the method

less attractive in real-life applications. Also, in several cases, the mean electron energy was overestimated by ERA [25].

Recently, Steuer *et al* [25] overcame some of the limitations of ERA by developing state enhanced actinometry (SEA) in which time and space integrated OES was used instead of PROES. Moreover, the helium emission line at the wavelength of 706.5 nm (He($3\,^3S \rightarrow 2\,^3P$)) was used instead of the 777.4 nm O emission line. SEA only required relatively simple measurements (compared to PROES), while the results for both the O density and the mean electron energy were in agreement with TALIF measurements and simulations. The trade-off is that helium emission lines need to be present in the plasma. This is not a problem for many APPs that operate in He feed gas, but if this is not the case, helium will need to be added as an actinometer gas similar to argon.

Despite the success of SEA, there are outstanding issues that our work aims to address. We aim to enhance the reliability and the accuracy of the SEA method, making it more widely applicable. First, Bayesian inference is applied for the determination of O density and mean electron energy from the actinometry model. The SEA method relies on finding the crossing points between the plotted lines from the two intensity ratios. A robust method for this is needed to obtain accurate results and importantly, quantifiable errors associated with the procedure. Second, the effect of cascading emission, de-excitation from higher states into the upper state of the line that is measured, is investigated. SEA does not take this process into account. Finally, SEA uses the 706.5 nm He emission line. However, there are concerns about the effects of the He metastable states on the upper state population of this transition. Alternatively, the use of the helium line at 728.1 nm (He($3\,^1S \rightarrow 2\,^1P$)) in our modified SEA method is investigated.

This paper is structured as follows: section 2 describes the plasma source, diagnostics and data analysis methods used in this work. Section 3 presents the results and discussions. The conclusion is in section 4.

2. Experimental setup and methods

2.1. Micro-scaled APP jet

The plasma source used in this work is a micro-scaled APP jet (μAPPJ) [26]. The electrode geometry and operating conditions of this device are identical to the widely used COST jet [2]. It is an APP device that consists of two parallel plane electrodes made of stainless steel, placed 1 mm apart. The sides of the electrodes are enclosed by quartz plates, forming a plasma channel 1 mm in width $\times$ 30 mm in length $\times$ 1 mm in height, as shown in figure 1.

A gas mixture of 1 slm He gas with admixtures of 0.5% O_2 (5 sccm) and 0.1% Ar (1 sccm) is flowing into the plasma channel. A radio-frequency (13.56 MHz) power supply is connected via an impedance-matching network to the powered electrode as shown in the schematic in figure 1.

Voltage and current are measured by a high-voltage probe (Tektronix P6015A: 1000x, 100 MHz, 20 kV) connected between the matching network and the electrode, and a current probe (Ion Physics Corp. CM-100-L: 1 V/A, 100 MHz, 20A), as shown in figure 1. Both the probes are connected to an oscilloscope (LeCroy WaveRunner 204MXi-A: 8 bit, 2 GHz, 10 GSa s^{-1}) to display and record the signals for analysis. The power dissipated in the plasma can be calculated from the measured voltage and current amplitudes and the phase shift between them, following the procedures set out by Golda *et al* [2]. The range of operating voltages achievable for the plasma, ranging from ignition to arcing, is 210–340 V_{rms}.

2.2. OES

Light emission from the μAPPJ is recorded by using two sensitivity-calibrated spectrometers (OceanOptics: HR4C4860 and OceanOptics: HR4C4667). The HR4C4860 is used to detect the optical range of 680–870 nm with the CCD array consisting of 3648 pixels ($\approx$0.05 nm per pixel) and the HR4C4667 covers the optical range of 196–1119 nm with the CCD array consisting of 3648 pixels ($\approx$0.3 nm per pixel). The integration times are varied from 300 ms up to 4 s, depending on operating conditions, ensuring a good signal-to-noise ratio. Each spectrometer is connected with its optical fibre (Ocean Optics QR600-2-SR; 600μm). Each optical fibre is positioned perpendicular to the plasma channel, halfway along the channel, with a distance of about 2 mm between the fibre and the quartz surface by a fixed lens mount while using each spectrometer. It has been shown in literature that the O density in μAPPJs reached an equilibrium before our measurement point for the plasma operating conditions that are used [27, 28].

Of interest for this work on actinometry are the emission lines at the wavelengths of 706.5, 728.1, 750.4 and 844.6 nm, corresponding to the transitions of He($3\,^3S \rightarrow 2\,^3P$), He($3\,^1S \rightarrow 2\,^1P$), Ar($2p_1 \rightarrow 1s_2$) and O($3p\,^3P \rightarrow 3s\,^3S$) respectively. Additionally, the transitions of He($3\,^3D \rightarrow 2\,^3P$) and He($3\,^1D \rightarrow 2\,^1P$) at the wavelengths of 587.6 and 667.8 nm are also of interest (see section 3.2). Figure 2 shows an example of a spectral profile for the plasma at 300 V_{rms}, highlighting the lines of interest for this work. With the resolution of HR4C4860, the nearby lines of Ar($2p_1 \rightarrow 1s_2$) and Ar($2p_5 \rightarrow 1s_4$) at the wavelengths of 750.4 and 751.5 nm respectively, can be resolved. Only the Ar($2p_1 \rightarrow 1s_2$) line is used in our method.

2.3. SEA

SEA was recently developed by Steuer *et al* [25]. It is used to measure atomic oxygen density in a plasma jet operated in He with O_2 admixtures and Ar as an actinometer gas. SEA uses two intensity ratios from the He($3\,^3S$) and O($3p\,^3P$) with Ar($2p_1$) upper excited states and gives the density of atomic oxygen and the mean electron energy of the plasma. SEA takes into account direct electron impact excitation of the

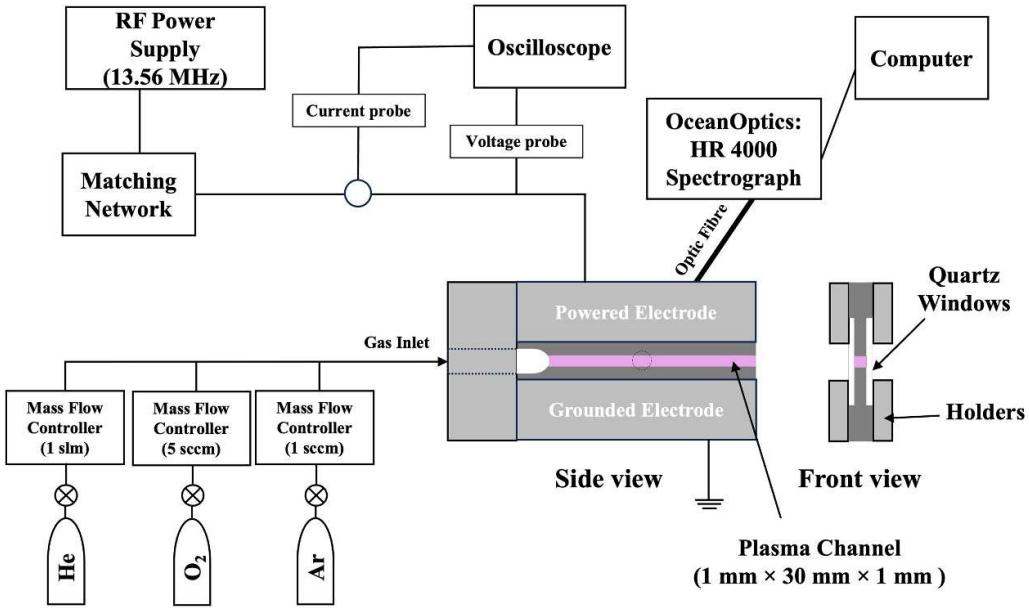

Figure 1. Schematic diagram of the μAPPJ plasma source.

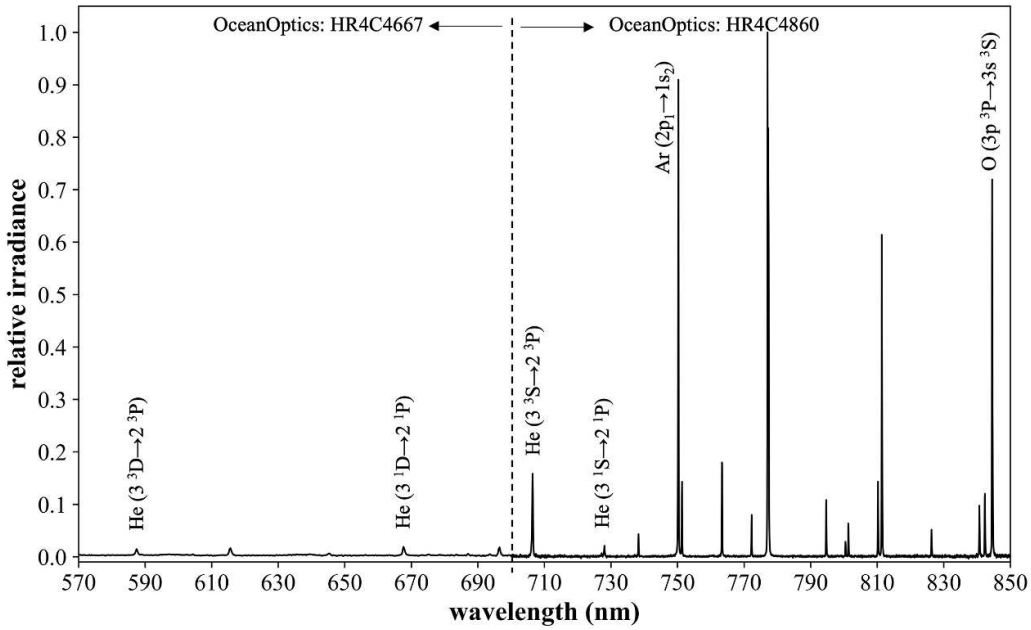

Figure 2. Example of a measured spectral profile from the spectrometers of HR4C4667 and HR4C4860. Operating conditions: the flow rates of 1 slm He + 5 sccm O_2 + 1 sccm Ar at the applied voltage of 300 V_{rms}, resulting in the power of about 1.30 W deposited in the plasma.

$O(3p\ ^3P)$ upper state from the ground state as well as dissociative electron impact excitation. The plasma is assumed to be optically thin. Full details can be found in Steuer *et al* [25]. The final equations for SEA, linking the measured intensity ratios $\frac{I_O^{(844.6)}}{I_{Ar}^{(750.4)}}$ and $\frac{I_{He}^{(706.5)}}{I_{Ar}^{(750.4)}}$ to the oxygen dissociation fraction (r_O), which can be related to the atomic oxygen density through the ideal gas law, and the mean electron energy (ε) are shown in equations (1) and (2).

$$\frac{I_O^{(844.6)}}{I_{Ar}^{(750.4)}} = \frac{f_{O_2}}{f_{Ar}} \frac{a_{ik,O}^{(844.6)}}{a_{ik,Ar}^{(750.4)}} \frac{\lambda_{Ar}^{(750.4)}}{\lambda_O^{(844.6)}} \frac{2r_O k_{d,O}^{(844.6)}(\varepsilon) + k_{de,O}^{(844.6)}(\varepsilon)}{k_{d,Ar}^{(750.4)}(\varepsilon)}, \tag{1}$$

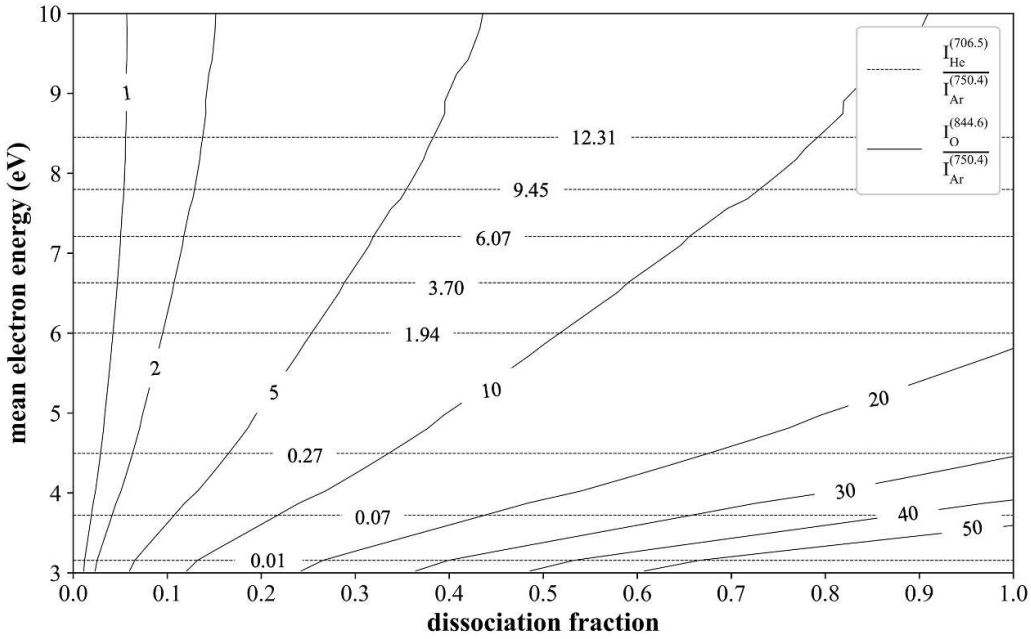

Figure 3. Example of the calculated intensity ratios as a function of the mean electron energy and the dissociation fraction. Experimental line ratios are mapped onto this figure to determine the plasma's dissociation fraction and mean electron energy.

$$\frac{I_{\mathrm{He}}^{(706.5)}}{I_{\mathrm{Ar}}^{(750.4)}} = \frac{f_{\mathrm{He}}}{f_{\mathrm{Ar}}} \frac{a_{ik,\mathrm{He}}^{(706.5)}}{a_{ik,\mathrm{Ar}}^{(750.4)}} \frac{\lambda_{\mathrm{Ar}}^{(750.4)}}{\lambda_{\mathrm{He}}^{(706.5)}} \frac{k_{d,\mathrm{He}}^{(706.5)}(\varepsilon)}{k_{d,\mathrm{Ar}}^{(750.4)}(\varepsilon)}. \tag{2}$$

where I is the integrated intensity of the emission line, the subscript refers to which atom is observed and the superscript to the observed wavelength. λ is the wavelength, f_{He}, f_{Ar} and $f_{\mathrm{O_2}}$ are the gas fractions of helium, argon and oxygen in the feed gas mixture, r_{O} is the dissociation fraction ($r_{\mathrm{O}} = \frac{\mathrm{n_O}}{2\mathrm{n_{O_2}}}$). Coefficients k are the energy-dependent effective reaction rates, calculated by the two-term approximation Boltzmann solver BOLSIG+ [24], and the indices d and de refer to direct electron impact excitation and dissociative electron impact excitation, respectively. Finally, a_{ik} is the effective branching ratio of the excited state.

The excited states of all species are depopulated by two processes: spontaneous emission to lower states and collisional induced quenching with background gas species. These two processes are incorporated in the form of the effective branching ratio of the excited state (a_{ik}) as follows:

$$a_{ik} = \frac{A_{ik}}{\sum_k A_{ik} + \sum_q k_q \mathrm{n}_q}. \tag{3}$$

where A_{ik} is the Einstein coefficient for spontaneous emission for the transition from an upper state i to a lower state k and taken from the NIST Atomic Spectra Database [29]. The term $\sum_k A_{ik}$ represents the decay into all possible lower states. This is the reciprocal of the natural lifetime (τ_i) of the upper level i and can be found in literature [12, 30, 31]. The term $\sum_q k_q \mathrm{n}_q$ is the total collisional induced quenching from background gas species q in a plasma (k_q and n_q are the quenching rate coefficient and the density of species q). The quenching rate coefficients for the Ar($2p_1$) and O($3p\ ^3P$) states from the background gas species can be found in literature [12, 31]. However, the quenching rate coefficients for the He($3\ ^3S$) state from the background gas species are unknown but it is found that the quenching rate coefficient from molecules is dominant when compared with that from atoms. For this reason, the quenching rate coefficient by hydrogen molecules is used for quenching by oxygen molecules for the He($3\ ^3S$) state [25], taken from [30].

For the calculation of the reaction rates (k), BOLSIG+ is input by a set of cross sections for He and O_2 from the LXcat database (S.F. Biagi's FORTRAN code, MagBoltz, versions 8.9 and later [32]). BOLSIG+ is set to consider a non-Maxwellian calculation, a reduced electric field (E/N) range of 5.7–70.0 Td ($\varepsilon \approx$ 3–10 eV) and a gas temperature of 330 K. The cross sections for direct and dissociative electron-impact excitation are taken from literature [33–35], using the same ones as ERA [23] for consistency. Since the expected dissociation in these plasmas is below 10%, the effects of this on the BOLSIG+ calculations of the reaction rates will be low. For simplicity, a constant gas composition of 99.5% He and 0.5% O_2 is used for all calculations.

Determination of atomic oxygen density from SEA comes from producing a graph of the intensity ratios for a range of mean electron energy and dissociation fractions as shown in figure 3.

The crossing point of the two measured intensity ratios then uniquely determines the mean electron energy and the dissociation fraction of the plasma. The atomic oxygen density can

be determined from the dissociation fraction using the density of molecular oxygen calculated from the ideal gas law by assuming a gas temperature of 330 K.

In the remainder of the paper, the method described in this section will be referred to as SEA(original).

2.4. Modified SEA

In this work, modifications to the SEA method, described in section 2.3, are made to include additional processes aimed at addressing outstanding issues of the SEA method. The first modification is considering cascading emission. Cascading emission is a population process of a given excited state from higher excited states. From literature, a cross section for only cascading emission can be found for the Ar($2p_1$) and O($3p\ ^3P$) upper states from [33] and [36] respectively but in the case of the He($3\ ^3S$) upper state, it is in the form of an apparent cross section which includes direct electron-impact excitation and cascading effects taken from [37]. As the result, the indices of *cc* and *ap* refer to cascading emission and apparent excitation respectively for this work. In the remainder of this paper, the modified method in which only cascading emission is added (using the original He emission line), is referred to as SEA(modified) as shown in equations (4) and (5).

Second, the emission from the He($3\ ^1S$) upper state at the wavelength of 728.1 nm is investigated instead of that from the He($3\ ^3S$) upper state which is used in SEA(original) because of the concern of population of the upper states from metastables. The original He($3\ ^3S$) state is in the triplet system of helium, which means that excitation from the ground state is spin-forbidden. Excitation of this level from the $2\ ^3S$ metastable state can be significant, which may be a problem for the SEA method. Emission from the He($3\ ^1S$) upper state at the wavelength of 728.1 nm is in the singlet system, reducing the issue of metastable excitation.

In the remainder of this paper, the method where the alternative emission line of helium is considered is referred to as SEA*(original) as shown in equations (6) and (7) while the method where both modifications are considered is referred to as SEA*(modified) as shown in equations (4) and (5).

With considering only cascading emission and both modifications, the governing equations become:

$$\frac{I_{\mathrm{O}}^{(844.6)}}{I_{\mathrm{Ar}}^{(750.4)}} = \frac{f_{\mathrm{O}_2}}{f_{\mathrm{Ar}}} \frac{a_{ik,\mathrm{O}}^{(844.6)}}{a_{ik,\mathrm{Ar}}^{(750.4)}} \frac{\lambda_{\mathrm{Ar}}^{(750.4)}}{\lambda_{\mathrm{O}}^{(844.6)}} \times \frac{2r_{\mathrm{O}}\left[k_{d,\mathrm{O}}^{(844.6)}(\varepsilon) + k_{cc,\mathrm{O}}^{(844.6)}(\varepsilon)\right] + k_{de,\mathrm{O}}^{(844.6)}(\varepsilon)}{k_{d,\mathrm{Ar}}^{(750.4)}(\varepsilon) + k_{cc,\mathrm{Ar}}^{(750.4)}(\varepsilon)}, \tag{4}$$

$$\frac{I_{\mathrm{He}}^{(706.5/728.1)}}{I_{\mathrm{Ar}}^{(750.4)}} = \frac{f_{\mathrm{He}}}{f_{\mathrm{Ar}}} \frac{a_{ik,\mathrm{He}}^{(706.5/728.1)}}{a_{ik,\mathrm{Ar}}^{(750.4)}} \frac{\lambda_{\mathrm{Ar}}^{(750.4)}}{\lambda_{\mathrm{He}}^{(706.5/728.1)}} \times \frac{k_{ap,\mathrm{He}}^{(706.5/728.1)}(\varepsilon)}{k_{d,\mathrm{Ar}}^{(750.4)}(\varepsilon) + k_{cc,\mathrm{Ar}}^{(750.4)}(\varepsilon)}. \tag{5}$$

With considering only the alternative He emission line, the governing equations become:

$$\frac{I_{\mathrm{O}}^{(844.6)}}{I_{\mathrm{Ar}}^{(750.4)}} = \frac{f_{\mathrm{O}_2}}{f_{\mathrm{Ar}}} \frac{a_{ik,\mathrm{O}}^{(844.6)}}{a_{ik,\mathrm{Ar}}^{(750.4)}} \frac{\lambda_{\mathrm{Ar}}^{(750.4)}}{\lambda_{\mathrm{O}}^{(844.6)}} \frac{2r_{\mathrm{O}}k_{d,\mathrm{O}}^{(844.6)}(\varepsilon) + k_{de,\mathrm{O}}^{(844.6)}(\varepsilon)}{k_{d,\mathrm{Ar}}^{(750.4)}(\varepsilon)}, \tag{6}$$

$$\frac{I_{\mathrm{He}}^{(728.1)}}{I_{\mathrm{Ar}}^{(750.4)}} = \frac{f_{\mathrm{He}}}{f_{\mathrm{Ar}}} \frac{a_{ik,\mathrm{He}}^{(728.1)}}{a_{ik,\mathrm{Ar}}^{(750.4)}} \frac{\lambda_{\mathrm{Ar}}^{(750.4)}}{\lambda_{\mathrm{He}}^{(728.1)}} \frac{k_{d,\mathrm{He}}^{(728.1)}(\varepsilon)}{k_{d,\mathrm{Ar}}^{(750.4)}(\varepsilon)}. \tag{7}$$

Other assumptions made in the SEA method, e.g. an optically thin plasma, are unchanged in our modified method.

Finally, finding a crossing point in figure 3 is a critical step in finding the dissociation fraction and mean electron energy. This is not straightforward since the measured intensity ratios can fall in between plotted ones so a (non-linear) interpolation procedure is needed. In the SEA work of Steuer *et al* [25], it is not clear what method is used for this. Here, we use Bayesian inference to determine the position of a crossing point, to ensure a robust and reliable method for more detail in appendix. Bayesian inference is commonly used for the estimation of parameter values, prediction of data values and model comparison [38, 39]. Bayesian methods are already applied to data analysis in different areas of plasma science, e.g. fusion [40], atomic physics [41], multi-diagnostic analysis for divertor plasma characteristics [42].

The general concept of Bayesian inference is that it assigns probabilities to parameters of interest from a model as compared with observed data, based on Bayes' theorem [43]. These probabilities can be continuously updated if more observed data is analysed along with prior knowledge [44, 45], as shown mathematically in equation (8).

$$P(\underline{\theta}|D) = \frac{P(D|\underline{\theta})\,P(\underline{\theta})}{P(D)}, \tag{8}$$

$$\text{with} \quad \underline{\theta} = [\theta_1, \theta_2, \ldots, \theta_n]$$

where $\underline{\theta}$ is the set of the parameters of interest, D is the observed data, $P(\underline{\theta})$ is the prior which is the initial probability before the observed data is analysed, $P(D|\underline{\theta})$ is the likelihood and is used for updating $P(\underline{\theta})$ due to the observed data from experimental measurements. In this work, Gaussian distributions are assumed. $P(\underline{\theta}|D)$ is the posterior, which is the probability of $\underline{\theta}$ given the observed data, that is, after the observed data is analysed and $P(D)$ is the evidence which is used for normalising the posterior ($P(D) = \sum_{\text{all}} P(D|\underline{\theta})P(\underline{\theta})$). It is noted that $P(D)$ is not necessary for parameter estimations, but is important when Bayesian inference is used for model comparison [39, 43].

$P(\underline{\theta}|D)$ is the probability of n parameters given D. In order to find the probability of a parameter of interest (θ_{interest}) given D, for example, $P(\theta_{\text{interest}}|D)$ can be calculated from the process of marginalisation as shown in equation (9). The probability from marginalisation of each parameter of interest is used to determine its mean value, including its credible interval.

$$P(\theta_{\text{interest}}|D) = \int_{-\infty}^{+\infty} \cdots \int_{-\infty}^{+\infty} P(\theta_{\text{interest}}, \theta_{\text{others}}|D)\, \mathrm{d}\theta_{\text{others}}. \tag{9}$$

3. Results and discussions

3.1. Effect of cascading emission

The plasma jet described in section 2 is operated with He gas with admixtures of 0.5% O_2 and 0.1% Ar. The plasma power is varied between 0.2 and 3.5 W and atomic oxygen density is derived from OES measurements as described in sections 2.3 and 2.4. The results for the SEA(original) and SEA(modified) methods are presented in figure 4, together with TALIF measurements from literature on the same plasma source [46]. The plasma power for the TALIF data was shifted by 1.1 W in figure 4 to match the ignition and arcing points of the SEA experiments since the methods for measuring plasma power were not the same for both investigations, leading to this offset.

Both SEA methods show an increasing trend in O density with plasma power, ranging from $2\times10^{21}\,\mathrm{m}^{-3}$ to $2.3\times10^{22}\,\mathrm{m}^{-3}$, in line with the TALIF measurements in literature. The modified SEA method, including the effects of cascading emission, results in a consistently increased density compared to the original SEA method by 40–60% approximately.

When SEA(original) and SEA(modified) are compared with TALIF from literature, the modified SEA gives a closer fit to the TALIF values, with the modified SEA O density higher for all plasma powers. However, it is important to note that both methods are within error of the TALIF results, making an evaluation about the accuracy of the SEA methods impossible.

Looking at experimental uncertainties in more detail, we note that the uncertainty in the TALIF results includes two different errors which are systematic errors and stochastic errors [46]. The systematic errors were about 53 %, dominated by the error in the two-photon absorption cross section ratio [46], while the stochastic errors were about 14 % for these measurements, leading to a total error of about 67% for the absolute O density measured with TALIF.

In case of the actinometry methods, Tsutsumi *et al* [47] suggested that the uncertainty for the O density using ERA should be at least 20%–30%. This uncertainty was based on the known uncertainties in the relevant cross sections.

In our work, the uncertainty of the O density from repeated experiments, which is calculated from Bayesian inference, is less than 1%, and negligible compared to other errors. The systematic uncertainty of the O density from the actinometry methods results from uncertainties in the literature values of the parameters in the models, related to the He($3\,^3S$), He($3\,^1S$), Ar($2p_1$) and O($3p\,^3P$) upper states. These parameters include cross sections, collisional quenching rates and natural lifetime as shown in table 1, where the accuracy of these parameters are estimated.

In order to estimate the uncertainty from our actinometry methods, we used a statistical approach by randomly selecting values, within their Gaussian uncertainties, for all the SEA parameters shown in table 1. These values are then used to calculate the O density and mean electron energy using the different SEA methods. This process is repeated a hundred times, with new values for the parameters every time, and the distributions of derived O density and mean electron energy are analysed to determine an estimate for the uncertainty. We find that for all SEA methods, the uncertainty for the derived O density is about 20%, as indicated in figures 4 and 6.

With these uncertainties, combined with the uncertainties of the TALIF results, it is impossible to determine which method is more accurate in determining O density. There is a need for more accurate data on cross sections, lifetimes and quenching coefficients, before the most appropriate SEA model can be derived. This work also provides a systematically-derived estimate for the uncertainty in the absolute values of O density measured with these SEA methods.

The second plasma parameter that is derived with SEA is mean electron energy. The mean electron energy as a function of plasma power is presented in figure 5. The uncertainty for the mean electron energy measured by the SEA methods is less than 3%, resulting from the statistical process as mentioned in the uncertainty for the derived O density. Therefore, the size of each error bar is smaller than that of each marker. It shows a similar, slightly increasing trend for both methods. The mean electron energy from SEA(modified) ranges from 6 to 8 eV as plasma power is increased between 0.2 and 3.5 W, while for SEA(original) the mean electron energy ranges from 4.5 to 6 eV. There is no direct comparison with other experimental methods available for the mean electron energy. However, Waskoenig *et al* [48] used simulation to determine the mean electron energy for a similar plasma and found it in the range of 2–3 eV. Some other actinometry-based methods also gave mean electron energy as outputs. For example, Greb *et al* [23] used ERA to determine the O density and the mean electron energy of a plasma similar to the one in this study. They found the mean electron energy in the range of 3–6 eV with increasing rf power. Steuer *et al* [25] reported the measurements in a COST jet, a plasma similar to the one in this study, in the range of 3–5 eV for SEA and 10–15 eV for ERA.

It is not possible to make a definitive assessment about the accuracy of the different methods, though it is clear that including cascading emission, as in the SEA(modified) method, makes a significant difference to the predicted mean electron energy. Based on a comparison with modelling, it seems the original SEA gives more realistic values for mean electron energy, even though these are still higher than expected from modelling.

3.2. Use of an alternative helium emission line

This section considers using the emission of the He($3\,^1S \rightarrow 2\,^1P$) transition at the wavelength of 728.1 nm instead of the He($3\,^3S \rightarrow 2\,^3P$) emission line at the wavelength of 706.5 nm to minimise the perturbing effects of excitation from metastable states.

The atomic oxygen density derived by using the 728.1 nm He emission line is shown in figure 6. SEA*(original) indicates the use of the 728.1 nm He emission line without

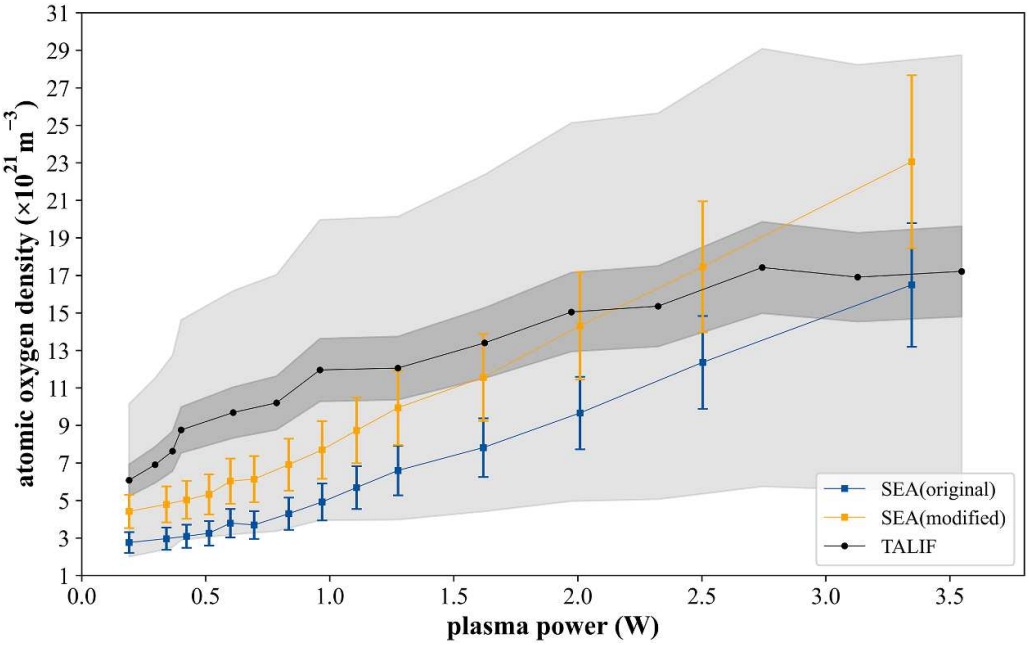

Figure 4. Atomic oxygen density derived by using the SEA(original) and SEA(modified) methods with 20% uncertainty (error bar) and TALIF measurements from literature [46] with a total estimated uncertainty of 67% (grey area) and a stochastic estimated uncertainty of 14% (dark area) [the assumed gas temperature of 330 K].

Table 1. Estimated uncertainties of each parameter from literature used in the SEA methods.

	Cross section (σ)				Quenching coefficient (k_q)		
Upper excited state	σ_d	σ_{de}	σ_{cc},σ_{ap}	Radiative lifetime (τ)	He	Ar	O_2
He($3\ ^3S$)	15%[b]	—	15%[b]	3%[30]	—	—	3%[30]
He($3\ ^1S$)	15%[b]	—	15%[b]	2%[30]	—	—	1%[30]
Ar($2p_1$)	20%[a][33]	—	15%[b]	8%[31]	30%[31]	10%[31]	10%[31]
O($3p\ ^3P$)	15%[b]	15%[35]	15%[b]	5%[12]	12%[12]	5%[12]	5%[12]

[a] The maximum uncertainty for $\sigma_{d,\mathrm{Ar}}$.
[b] Estimate based on $\sigma_{de,\mathrm{O}}$.

cascading emission, while SEA*(modified) includes both cascading emission and the 728.1 nm He emission line. The data from figure 4 for SEA(original) and SEA(modified), highlighting the effect on only cascading emission, is also included in figure 6 for comparison.

The atomic oxygen density in figure 6 shows that both the SEA* methods give O density lower than the SEA methods, indicating that considering the 728.1 nm He emission line consistently leads to lower density. It is not immediately clear whether this lower density is a result of uncertainties in excitation cross-sections, or due to excitation from metastable states. The differences between the SEA and SEA* methods could be due to uncertainties in the cross sections, lifetimes and quenching coefficients that are needed for the different lines. This is highlighted by the fact that the SEA and SEA* methods are within error of each other for all measurements (see figure 6). This means that even though considering the alternative He emission line does change the O density by 20%–40% approximately, it not possible to be sure that this is an improvement due to a lower impact of excitation from metastable states, rather than a difference due to the accuracy of the necessary input data.

As an alternative analysis, Raud *et al* [49] proposed a way to establish the dominant excitation pathway, e.g. electron impact from the ground state or from metastable states, by comparing the intensities of He($3\ ^1D \rightarrow 2\ ^1P$) and He($3\ ^3D \rightarrow 2\ ^3P$) transitions at the wavelengths of 667.8 and 587.6 nm, respectively.

If the excitation is only from the ground state, then the ratio of the He($3\ ^1D \rightarrow 2\ ^1P$) and He($3\ ^3D \rightarrow 2\ ^3P$) emission intensities can be calculated from the relevant cross sections [50] and radiative transition properties [29] for a given EEDF. It is found that the intensity ratio is fairly constant at 1.8 approximately for EEDFs in the range of 3–8 eV.

For excitation of the upper levels from the He($2\ ^1S$) and He($2\ ^3S$) metastable states, the ratio of reaction rates is also about 1.8, for the same range of EEDFs [50]. So any change away from 1.8 for the intensity ratio of 667.8 nm and 587.6 nm, is a result of a difference in density between the He($2\ ^1S$) and He($2\ ^3S$) metastable states, and indicates a significant contribution of excitation of the metastable states to the overall density of the He($3\ ^1D$) and He($3\ ^3D$) upper states.

The density of the triplet metastable state, He($2\ ^3S$), is expected to be higher than that of the singlet metastable state,

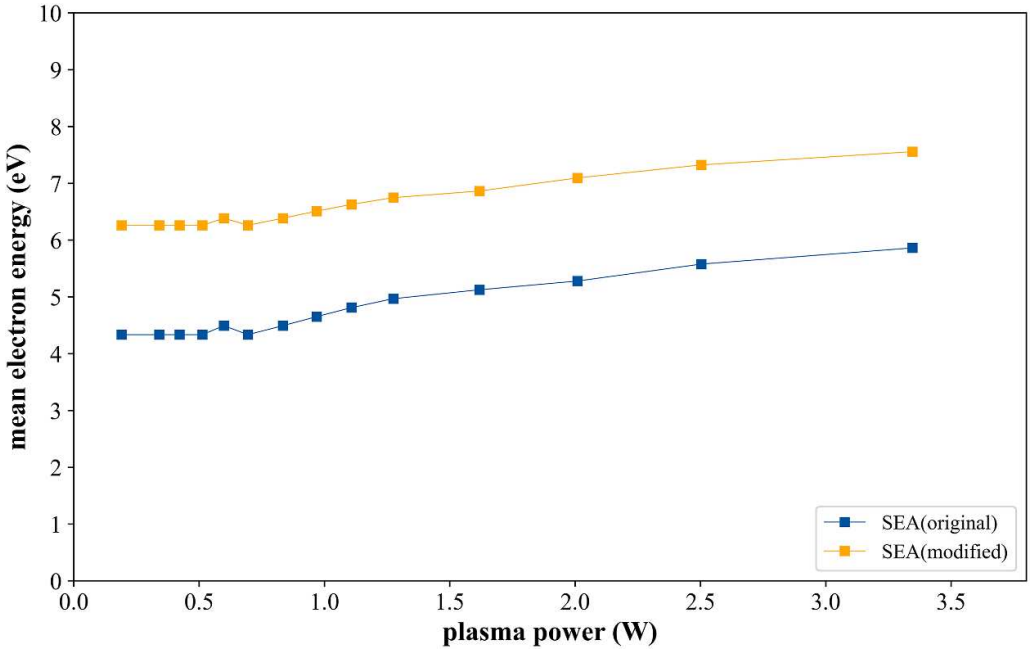

Figure 5. Calculated mean electron energy from the SEA(original) and SEA(modified) methods.

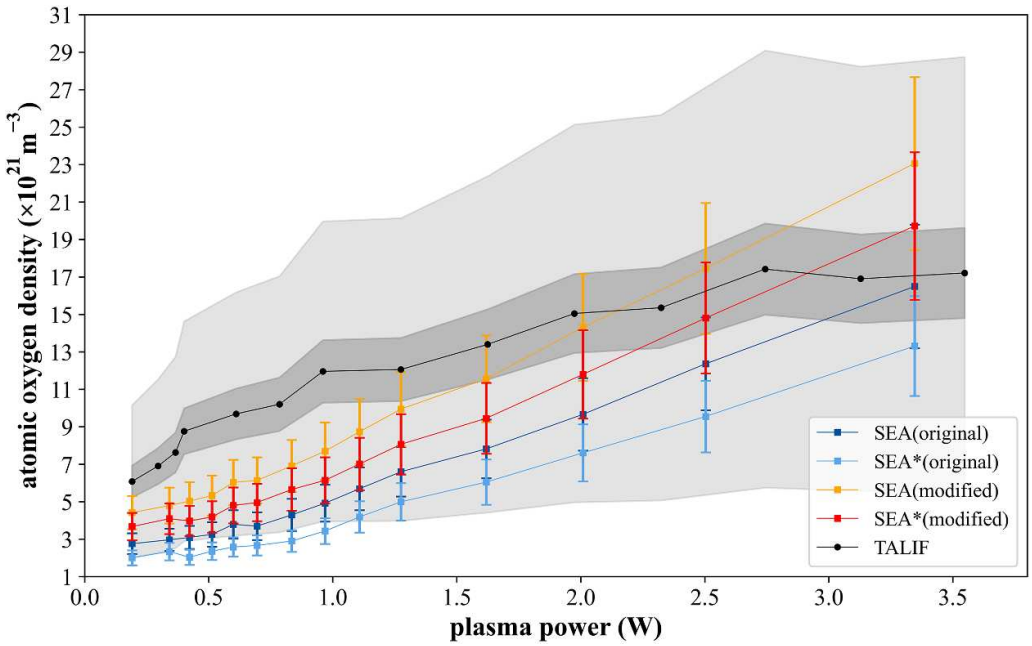

Figure 6. Atomic oxygen density derived by using the SEA(original), SEA*(original), SEA(modified) and SEA*(modified) methods with 20% uncertainty (error bar) and TALIF measurements from literature [46] with the total estimated uncertainty of 67% (grey area) and the stochastic estimated uncertainty of 14% (dark area) (the assumed gas temperature of 330 K).

$He(2\ ^1S)$, because of an efficient conversion channel of superelastic collisions of the singlet metastable state with thermal electrons [51]. This will lead to an increase in $He(3\ ^3D)$ density, therefore an increase in 587.6 nm emission, leading to a lower ratio of 667.8 and 587.6 nm.

The intensity ratio of the $He(3\ ^1D \rightarrow 2\ ^1P)$ and $He(3\ ^3D \rightarrow 2\ ^3P)$ transitions at the wavelengths of 667.8 nm and 587.6 nm measured in our work is shown in figure 7. It shows that the intensity ratio is approximately 1.5 for applied voltages of 275 V_{rms} and over. This ratio is lower than 1.8, which is what can be expected from the ground-state excitation alone, indicating that even though the situation is dominated by the ground-state excitation, there is a significant contribution of excitation from metastable states for voltages over 275 V_{rms}. Quantifying the contribution requires knowledge of (the ratio of) the density of the singlet and triplet metastables. Nevertheless, this result suggests that there is a contribution of excitation from the metastable states and therefore the use

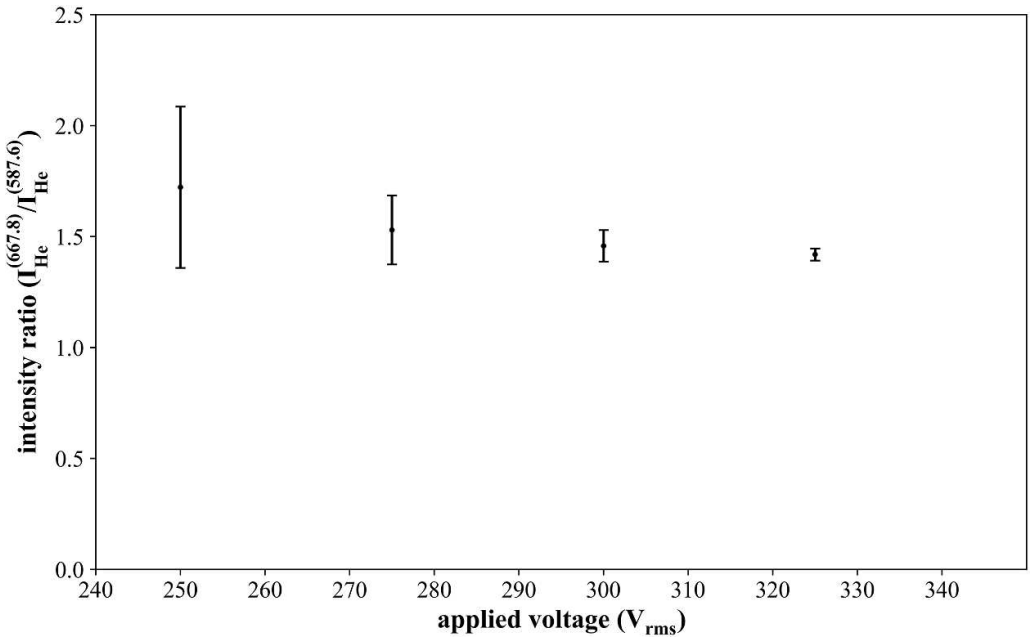

Figure 7. Measured intensity ratio between He($3\ ^1D \rightarrow 2\ ^1P$) and He($3\ ^3D \rightarrow 2\ ^3P$) transitions at the wavelengths of 667.8 nm and 587.6 nm.

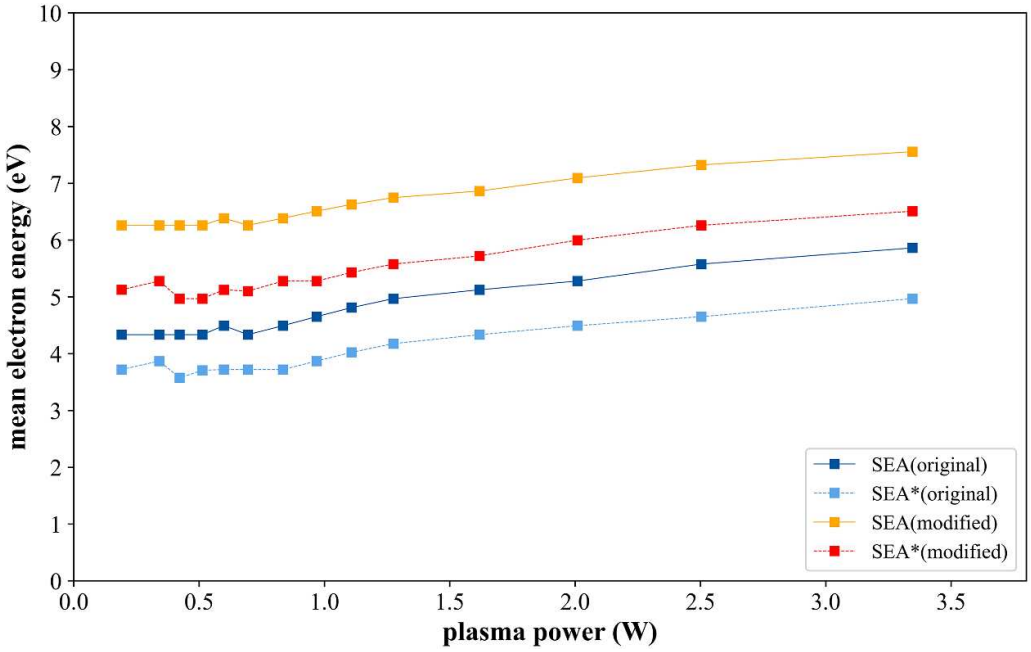

Figure 8. Calculated mean electron energy from the SEA(original), SEA*(original), SEA(modified) and SEA*(modified) methods.

of the 728.1 nm He emission line in the SEA* methods are indeed an improvement of the model and not only a difference due to available literature data.

A further consideration is the possible effect of radiation trapping of 58.4 nm light from the transition between the He($2\ ^1P$) state and the ground state. The high density of the He($2\ ^1P$) state would lead to enhanced excitation of the He($3\ ^1D$) and He($3\ ^3D$) upper states. The cross sections in [50] show that the electron-impact excitation from the He($2\ ^1P$) state to the He($3\ ^1D$) upper state is more likely than to the He($3\ ^3D$) upper state by several orders of magnitude. Therefore, if the population of the He($2\ ^1P$) state would be significant, the intensity ratio of 667.8 and 587.6 nm would be higher than 1.8, not lower. This suggests that radiation trapping of the 58.4 nm light to the He($2\ ^1P$) state is not a significant process under these plasma conditions.

The results for mean electron energy are shown in figure 8. It can be seen that the mean electron energy is lower for the SEA* methods compared to the SEA methods by roughly 1 eV for all plasma power. It seems that considering the alternative

728.1 nm He emission line brings the mean electron energy closer to that from modelling, though similar to the O density, it is not fully certain that this is because of a reduction of the perturbation of metastable excitation or a more accurate cross section.

Finally, it should be noted that the difference between the SEA(original) and SEA*(modified), with both modifications included, is relatively minor, in the range of 20%–40% approximately due to the fact that the changes in O density due to the modifications are in opposite directions, somewhat cancelling each other out.

4. Conclusion

Modifying the SEA method by including cascading emission and an alternative He emission line does significantly change the calculated O density by about 40%–60% when considering only cascading emission, and about 20%–40% for both modifications. However, due to the lack of accurate data on the real O density, it is impossible to establish the most accurate method. Interestingly, the effects of both modifications partially cancel out for the conditions in this work. This investigation highlights the limitations in accuracy of the SEA methods, finding an uncertainty of about 20% for any measurement. This is mainly due to the lack of more accurate input data for cross sections, lifetimes and quenching coefficients. Improvements in the accuracy of these values will need to be made before further investigations into the optimal SEA model can be done. Of course, it is important to note that these findings are applicable to the specific plasma used in this study, but generalisation of the methods to other plasma systems has not been considered.

Data availability statement

The data that support the findings of this study are openly available at the following URL/DOI: https://doi.org/10.15124/9ea4fe46-9776-4030-87b6-fe8feda2d784.

Acknowledgment

K Poonsawat acknowledges financial support from the Development and Promotion of Science and Technology Talents Project (DPST), Royal Government of Thailand scholarship.

Appendix

Bayesian inference procedures to determine O density (via a dissociation fraction) and mean electron energy (via reaction rates) out of the equations from each SEA model used in this work will be shown in this appendix. According to equation (8), Bayesian inference is shown in the mathematical equation for the estimations of parameters. The parameters of interest for this work in each SEA model are the dissociation fraction (r_O) and mean electron energy (ϵ). Therefore, equation (8) will be applied for this work to become as follows:

$$P(r_O,\epsilon|D_1,D_2)=\frac{P(D_1,D_2|r_O,\epsilon)P(r_O,\epsilon)}{P(D_1,D_2)}. \tag{A.1}$$

where r_O and ϵ are the parameters of interest, D_1 and D_2 are the observed data from the measured intensity ratios of $\frac{I_O^{(844.6)}}{I_{Ar}^{(750.4)}}$ and $\frac{I_{He}^{(706.5/728.1)}}{I_{Ar}^{(750.4)}}$ respectively, $P(r_O,\epsilon)$ is the prior which is the initial probability before the observed data is analysed, $P(D_1,D_2|r_O,\epsilon)$ is the likelihood and is used for updating $P(r_O,\epsilon)$ due to the observed data from experimental measurements, $P(r_O,\epsilon|D_1,D_2)$ is the posterior, which is the probability of r_O and ϵ given the observed data, that is, after the observed data is analysed and $P(D_1,D_2)$ is the evidence which is used for normalising the posterior, which is not necessarily considered for parameter estimations.

From equation (A.1), it can be arranged to be in a new form as follows:

$$P(r_O,\epsilon|D_1,D_2)=\frac{P(D_1|r_O,\epsilon)P(D_2|r_O,\epsilon)P(r_O)P(\epsilon)}{P(D_1,D_2)}. \tag{A.2}$$

In this case, $P(r_O)$ and $P(\epsilon)$ were chosen to be uniform in the given ranges of r_O and ϵ. The experiments measure the intensity ratios of $\frac{I_O^{(844.6)}}{I_{Ar}^{(750.4)}}$ and $\frac{I_{He}^{(706.5/728.1)}}{I_{Ar}^{(750.4)}}$ distorted by Gaussian noise of known variance σ^2. Therefore, the likelihoods are then given by

$$P(D_1|r_O,\epsilon)=\frac{1}{\sigma_1\sqrt{2\pi}}\exp\left(-\frac{1}{2}\left(\frac{D_1-f_1(r_O,\epsilon)}{\sigma_1}\right)^2\right), \tag{A.3}$$

and

$$P(D_2|r_O,\epsilon)=\frac{1}{\sigma_2\sqrt{2\pi}}\exp\left(-\frac{1}{2}\left(\frac{D_2-f_2(r_O,\epsilon)}{\sigma_2}\right)^2\right). \tag{A.4}$$

where $f_1(r_O,\epsilon)$ and $f_2(r_O,\epsilon)$ are the functions to predict $\frac{I_O^{(844.6)}}{I_{Ar}^{(750.4)}}$ and $\frac{I_{He}^{(706.5/728.1)}}{I_{Ar}^{(750.4)}}$ from each SEA model.

It is noted that the evidence ($P(D_1,D_2)$) is ignored in this work as not necessary for parameter estimations [39, 43]. For the computational process, the natural logarithm is used for equation (A.2) to calculate the posterior ($P(r_O,\epsilon|D_1,D_2)$).

$P(r_O,\epsilon|D_1,D_2)$ is the probability of r_O and ϵ given D_1 and D_2. In order to find the probability of r_O or ϵ given D_1 and D_2, the process of marginalisation as shown in equation (9) is needed. Therefore, $P(r_O|D_1,D_2)$ is given by

$$P(r_O|D_1,D_2)=\int_{\epsilon_{min}}^{\epsilon_{max}}P(r_O,\epsilon|D_1,D_2)\,d\epsilon, \tag{A.5}$$

and $P(\epsilon|D_1,D_2)$ is given by

$$P(\epsilon|D_1,D_2)=\int_{r_{O_{min}}}^{r_{O_{max}}}P(r_O,\epsilon|D_1,D_2)\,dr_O. \tag{A.6}$$

The probability from marginalisation of each parameter of interest is normalised and can be used to determine its mean value, including its credible interval

ORCID iDs

Kittawat Poonsawat 0000-0001-8924-3866
Erik Wagenaars 0000-0002-5493-3434

References

[1] Schröder D, Bahre H, Knake N, Winter J, Arcos T D L and Schulz-Von Der V 2012 Influence of target surfaces on the atomic oxygen distribution in the effluent of a micro-scaled atmospheric pressure plasma jet *Plasma Sources Sci. Technol.* **21** 024007
[2] Golda J *et al* 2016 Concepts and characteristics of the 'cost reference microplasma jet *J. Phys. D: Appl. Phys.* **49** 084003
[3] Ionita M D *et al* 2010 Surface modification of polymers at atmospheric pressure in expanding rf plasmas generated by planar dielectric barrier discharges *J. Optoelectron. Adv. Mater.* **12** 777–82 (available at: https://joam.inoe.ro/articles/surface-modification-of-polymers-at-atmospheric-pressure-in-expanding-rf-plasmas-generated-by-planar-dielectric-barrier-discharges/fulltext)
[4] Hefny M M, Nečas D, Zajíčková L and Benedikt J 2019 The transport and surface reactivity of o atoms during the atmospheric plasma etching of hydrogenated amorphous carbon films *Plasma Sources Sci. Technol.* **28** 035010
[5] Shaw D, West A, Bredin J and Wagenaars E 2016 Mechanisms behind surface modification of polypropylene film using an atmospheric-pressure plasma jet *Plasma Sources Sci. Technol.* **25** 065018
[6] Sarangapani C, O'Toole G, Cullen P J and Bourke P 2017 Atmospheric cold plasma dissipation efficiency of agrochemicals on blueberries *Innov. Food Sci. Emerg. Technol.* **44** 235–41
[7] Lei X, Yepez X, Applegate B, Keener K M, Tao B and Garner A L 2020 Penetration and microbial inactivation by high voltage atmospheric cold plasma in semi-solid material *Food Bioprocess Technol.* **13** 1688–702
[8] Gay-Mimbrera J, García M C, Isla-Tejera B, Rodero-Serrano A, Vélez García-Nieto A and Ruano J 2016 Clinical and biological principles of cold atmospheric plasma application in skin cancer *Adv. Ther.* **33** 894–909
[9] Bernhardt T, Semmler M L, Schäfer M, Bekeschus S, Emmert S and Boeckmann L 2019 Plasma medicine: applications of cold atmospheric pressure plasma in dermatology *Oxid. Med. Cell. Longevity* **2019** 3873928
[10] West A, van der Schans M, Xu C, Cooke M and Wagenaars E 2016 Fast, downstream removal of photoresist using reactive oxygen species from the effluent of an atmospheric pressure plasma jet *Plasma Sources Sci. Technol.* **25** 02LT01
[11] Schröter A *et al* 2018 Chemical kinetics in an atmospheric pressure helium plasma containing humidity *Phys. Chem. Chem. Phys.* **20** 24263–86
[12] Niemi K, Schulz-Von Der Gathen V and Döbele H F 2005 Absolute atomic oxygen density measurements by two-photon absorption laser-induced fluorescence spectroscopy in an rf-excited atmospheric pressure plasma jet *Plasma Sources Sci. Technol.* **14** 375
[13] Knake N, Reuter S, Niemi K, Schulz-Von Der Gathen V and Winter J 2008 Absolute atomic oxygen density distributions in the effluent of a microscale atmospheric pressure plasma jet *J. Phys. D: Appl. Phys.* **41** 194006
[14] Schröter S, Bredin Jôme, Gibson A R, West A, Dedrick J P, Wagenaars E, Niemi K, Gans T and O'Connell D 2020 The formation of atomic oxygen and hydrogen in atmospheric pressure plasmas containing humidity: picosecond two-photon absorption laser induced fluorescence and numerical simulations *Plasma Sources Sci. Technol.* **29** 105001
[15] Brisset A, Bieniek M, Invernizzi L, Hasan M, Walsh J, Niemi K and Wagenaars E 2023 The formation of o and h radicals in a pulsed discharge in atmospheric pressure helium with water vapour admixtures *Plasma Sources Sci. Technol.* **32** 065004
[16] Coburn J W and Chen M 1980 Optical emission spectroscopy of reactive plasmas: a method for correlating emission intensities to reactive particle density *J. Appl. Phys.* **51** 3134–6
[17] Walkup R E, Saenger K L and Selwyn G S 1986 Studies of atomic oxygen in o_{2+} cf_4 rf discharges by two-photon laser-induced fluorescence and optical emission spectroscopy *J. Chem. Phys.* **84** 2668–74
[18] Katsch H M, Tewes A, Quandt E, Goehlich A, Kawetzki T and Döbele H F 2000 Detection of atomic oxygen: improvement of actinometry and comparison with laser spectroscopy *J. Appl. Phys.* **88** 6232–8
[19] Niemi K, Stephan Reuter L M G, Waskoenig J and Gans T 2009 Diagnostic based modeling for determining absolute atomic oxygen densities in atmospheric pressure helium-oxygen plasmas *Appl. Phys. Lett.* **95** 151504
[20] Niemi K, Stephan Reuter L M G, Waskoenig J, Knake N, Schulz-Von Der Gathen V and Gans T 2010 Diagnostic based modelling of radio-frequency driven atmospheric pressure plasmas *J. Phys. D: Appl. Phys.* **43** 124006
[21] Sakiyama Y and Graves D B 2006 Corona-glow transition in the atmospheric pressure rf-excited plasma needle *J. Phys. D: Appl. Phys.* **39** 3644
[22] Schulze J, Schüngel E, Donkó Z, Luggenhölscher D and Czarnetzki U 2010 Phase resolved optical emission spectroscopy: a non-intrusive diagnostic to study electron dynamics in capacitive radio frequency discharges *J. Phys. D: Appl. Phys.* **43** 124016
[23] Greb A, Niemi K, O'Connell D and Gans T 2014 Energy resolved actinometry for simultaneous measurement of atomic oxygen densities and local mean electron energies in radio-frequency driven plasmas *Appl. Phys. Lett.* **105** 234105
[24] Hagelaar G J M and Pitchford L C 2005 Solving the boltzmann equation to obtain electron transport coefficients and rate coefficients for fluid models *Plasma Sources Sci. Technol.* **14** 722
[25] Steuer D, van Impel H, Gibson A R, Schulz-Von Der Gathen V, Böke M and Golda J 2022 State enhanced actinometry in the cost microplasma jet *Plasma Sources Sci. Technol.* **31** 10LT01
[26] Schulz-von der Gathen V, Buck V, Gans T, Niemi K, Reuter S, Schaper L and Winter J 2007 Optical diagnostics of micro discharge jets *Contrib. Plasma Phys* **47** 510–9
[27] Knake N, Niemi K, Reuter S, Schulz-Von Der Gathen V and Winter J 2008 Absolute atomic oxygen density profiles in the discharge core of a microscale atmospheric pressure plasma jet *Appl. Phys. Lett.* **93** 131503
[28] Knake N and Schulz-Von Der Gathen V 2010 Investigations of the spatio-temporal build-up of atomic oxygen inside the micro-scaled atmospheric pressure plasma jet *Eur. Phys. J. D* **60** 645–52
[29] Nist atomic spectra database lines form (available at: https://physics.nist.gov/PhysRefData/ASD/lines_form.html) (Accessed 21 February 2023)

[30] Gans T, Lin C C, Schulz-Von Der Gathen V and Döbele H F 2003 Phase-resolved emission spectroscopy of a hydrogen rf discharge for the determination of quenching coefficients *Phys. Rev. A* **67** 012707
[31] Sadeghi N, Setser D W, Francis A, Czarnetzki U and Döbele H F 2001 Quenching rate constants for reactions of Ar (4p [1/2], 4p [1/2], 4p [3/2] 2 and 4p [5/2] 2) atoms with 22 reagent gases *J. Chem. Phys.* **115** 3144–54
[32] S F Biagi's fortran code, magboltz, versions 8.9 and later (available at: www.lxcat.net/Biagi) (Accessed 25 July 2023)
[33] Chilton J E, Boffard J B, Schappe R S and Lin C C 1998 Measurement of electron-impact excitation into the 3 p 5 4 p levels of argon using Fourier-transform spectroscopy *Phys. Rev. A* **57** 267
[34] Laher R R and Gilmore F R 1990 Updated excitation and ionization cross sections for electron impact on atomic oxygen *J. Phys. Chem. Ref. Data* **19** 277–305
[35] Schulman M B, Sharpton F A, Chung S, Lin C C and Anderson L W 1985 Emission from oxygen atoms produced by electron-impact dissociative excitation of oxygen molecules *Phys. Rev. A* **32** 2100
[36] Caplinger J E and Perram G P 2020 The importance of cascade emission and metastable excitation in modeling strong atomic oxygen lines in laboratory plasmas *Plasma Sources Sci. Technol.* **29** 015011
[37] John R M S, Miller F L and Lin C C 1964 Absolute electron excitation cross sections of Helium *Phys. Rev.* **134** A888
[38] Kruschke J 2014 *Doing Bayesian Data Analysis: A Tutorial With R, Jags and Stan* (Academic) (https://doi.org/10.1016/B978-0-12-405888-0.09999-2)
[39] Toussaint U V 2011 Bayesian inference in physics *Rev. Mod. Phys.* **83** 943
[40] Bowman C 2016 Applications of Bayesian probability theory in fusion data analysis *PhD Thesis* University of York (available at: https://etheses.whiterose.ac.uk/id/eprint/16978/)
[41] Trassinelli M 2020 An introduction to Bayesian statistics for atomic physicists *J. Phys.: Conf. Ser.* **1412** 062008
[42] Bowman C, Harrison J R, Lipschultz B, Simon Orchard K J G, Carr M, Verhaegh K and Myatra O 2020 Development and simulation of multi-diagnostic Bayesian analysis for 2D inference of divertor plasma characteristics *Plasma Phys. Control. Fusion* **62** 045014
[43] Sivia D and Skilling J 2006 *Data Analysis: a Bayesian Tutorial* (OUP Oxford)
[44] Lambert B 2018 A student's guide to Bayesian statistics *A Student's Guide to Bayesian Statistics* pp 1–520
[45] Fornacon-Wood I, Mistry H, Johnson-Hart C, Faivre-Finn C, O'Connor J P B and Price G J 2022 Understanding the differences between Bayesian and frequentist statistics *Int. J. Rad. Oncol. Biol. Phys.* **112** 1076–82
[46] West A 2016 Optical and electrical diagnosis of atmospheric pressure plasma jets *PhD Thesis* University of York (available at: https://etheses.whiterose.ac.uk/id/eprint/15199/)
[47] Tsutsumi T, Greb A, Gibson A R, Hori M, O'Connell D and Gans T 2017 Investigation of the radially resolved oxygen dissociation degree and local mean electron energy in oxygen plasmas in contact with different surface materials *J. Appl. Phys.* **121** 143301
[48] Waskoenig J, Niemi K, Knake N, Graham L M, Reuter S, Schulz-Von Der Gathen V and Gans T 2010 Atomic oxygen formation in a radio-frequency driven micro-atmospheric pressure plasma jet *Plasma Sources Sci. Technol.* **19** 045018
[49] Raud J and Laan M 2008 Positive column of hf discharge in he/n2 mixture: excitation and ionization mechanisms *J. Phys. D: Appl. Phys.* **42** 015205
[50] Ralchenko Y, Janev R K, Kato T, Fursa D V, Bray I and de Heer F J 2008 Electron-impact excitation and ionization cross sections for ground state and excited helium atoms *At. Data Nucl. Data Tables* **94** 603–22
[51] Korolov I *et al* 2020 Helium metastable species generation in atmospheric pressure rf plasma jets driven by tailored voltage waveforms in mixtures of he and n2 *J. Phys. D: Appl. Phys.* **53** 185201